Superior Piecewise Logistic Map with Chaos Control

Dildar Husain, Mamta Rani

***Abstract*—The superior (Mann) iteration method has been used in fractals and chaos. The study iterated the piecewise logistic map in this research article via a superior iteration method. The present study has analyzed the superior piecewise logistic map through the time series plotting method, density distribution function, Lyapunov function, and bifurcation diagram to testify that it gives better results than existing chaotic maps. Parrondo's paradox concept has also been used to determine that chaos^1 + chaos^2 = order or order^1 + order^2 = chaos.**

***Index Terms*—Piecewise Logistic Map, Time Series Plot, Parrondo's Paradox, Lyapunov Exponent, Alternate System, Periodic Window Glitch, Bifurcation.**

I. Introduction

The iterated logistic map is the foundation of chaos theory. Controlling the chaotic situation in non-linear models has been challenging. Parrondos's paradox [1] suggested iterating the two logistic maps alternatively, which gave the concept of "chaos^1 + chaos^2 = order" (chaos control). Also, the idea of order^1 + order^2 = chaos" or "chaos^1 + order^1 = chaos" (chaos anti-control) was given [2].

Chaotic maps are used in many places, such as to generate pseudo-random numbers [3], random bits [17], global search optimization algorithms for swarm particles [5][6], and in cryptosystems such as audio encryption [7], video encryption [8], image encryption [9][10][11][12], text encryption [13], etc. On the other hand, a piecewise logistic map (PLM), an enhanced version of the logistic map has better cryptographic properties like robustness, efficiency, higher entropy, and higher security than other chaotic maps [14][18].

FAN Jiu-lun and ZHANG Xue-Feng [16] have generated PLM-based sequences that contain randomness. Further, Ali Kanso and Nejib Smaoui [17] also used PLM to generate a binary key stream with an extended period length, better statistical properties, and high linear complexity, which is hard to predict.

Yong Wang et al. [18] presented a PLM-based pseudo-random number generator (PRNG) with enhanced security as compared to a logistic map. Dragan Lambic [14] analyzed the security of PLM-based PRNG and proved that PRNG is unsafe for use in cryptography. Due to the lack of uniform distribution in PLM, Wang et al. [19] designed Parameterized Coupled PLM that achieved the uniform distribution and proposed PRNG. The proposed scheme has multi-positive Lyapunov exponents, have higher entropy, and is more efficient.

To overcome the shortcomings of earlier approaches specified over real numbers, Sota Eguchi et. al, [20] investigates a pseudorandom number generator employing a piecewise logistic map over integers. The range of control parameters is increased by raising the number of divisions m, which maintains output variability and improves unpredictability. It is a good substitute for conventional logistic maps, as demonstrated by numerical studies that show enhanced performance in terms of Lyapunov exponent, period, link length, and NIST test results.

Xiang et al. [21] implemented PLM to perform a chaotic search with particle swarm optimization known as PW-LCPSO. This proposed method is compared numerically with the existing CPSO algorithm and is superior in robustness and efficiency.

Jia and Wang [22] used PLM in place of the logistic map in a Globally coupled neural network chaotic map (GCM) is used to explore chaos control and dynamics mechanisms. Feedback control controls the specified periodic orbit of delay coupling or conventional coupling. Using this controlling technique, they have shown that the GCM network is managed successfully.

The paper has implemented a superior iteration of the PLM of the dynamical system with the control of Parrondo's paradox (a switching strategy) used to determine the desired outcome. Our proposed work may be used in many places, such as in chaotic cryptography (image encryption, text encryption, audio encryption, etc.), pseudo-random number generation, or the multi-scaled population in the superior orbit.

The organization of the paper is as follows. Section II has given some definitions of what is used in this article. In section III, we have done some analysis to check the stability, periodicity, and instability of SPLM and presented them graphically. Section IV describes the exception's existence in SPLM. Section V contains the details about the density probability distribution of SPLM. In Section VI, we have presented the sensitivity of SPLM through the diagram of parameterized Lyapunov exponents. Section VII shows the paramterized bifurcation of SPLM. Section VIII provided chaos control for the SPLM; Section IX presented the findings of the NIST Test applied to the pseudo-random number generated by the SPLM, and Section IX marked the article's conclusion.

II. Preliminaries

Definition 2.1: Piecewise Logistic Map (PLM) [18]
The Piecewise logistic map is defined as (Equ.-1)

Manuscript received July 10, 2024; revised March 5, 2025.

Dildar Husain is a Research Scholar at the Department of Computer Science, Central University of Rajasthan, Dist-Ajmer, 305817, Rajasthan, India (corresponding author to provide email: todildar@outlook.com).

Mamta Rani is a Professor at the Department of Computer Science, Central University of Rajasthan, Dist-Ajmer, 305817, Rajasthan, India (e-mail: mamtarsingh@curaj.ac.in).

The function $F_c : f(x_n, \mu) = x_{n+1}$ is defined as:

$$x_{n+1} = \begin{cases} N^2\mu\left(x_n - \frac{i-1}{N}\right)\left(\frac{i}{N} - x_n\right), & \text{for } \frac{i-1}{N} < x_n < \frac{i}{N}, \\ (1-N)^2\mu\left(x_n - \frac{i-1}{N}\right)\left(\frac{i}{N} - x_n\right), & \text{for } \frac{i}{N} < x_n < \frac{i+1}{N}, \\ x_n + \frac{1}{100N}, & \text{for } x_n = 0, \frac{1}{N}, \frac{2}{N}, \ldots, \frac{N-1}{N}, \\ x_n - \frac{1}{100N}, & \text{for } x_n = 1. \end{cases} \tag{1}$$

Definition 2.2: Peano-Picard Iteration [23]
Let R be a non-empty subset of real numbers on a metric space, and $R : X \to X$. For a point x_0 in X, the Picard orbit (generally called the orbit) of f is the set of all iterates of the point x_0, that is:

$$O(f, x_0) = \{x_n : x_n = f(x_{n-1}), n = 1, 2, 3, \ldots\}$$

The orbit of f at the initial point x_0, $O(f, x_0)$, is the sequence $\{f^n(x_0)\}$.

Definition 2.3: Superior (Mann) Iteration [24]
Let X be a linear space, T a convex subset of X, and let $X : T \to T$ be a mapping and $x_1 \in C$, arbitrary. Let $A = [a_{jn}]$ be an infinite real matrix satisfying:

(A1) $a_{jn} \geq 0$ for all n, j and $a_{jn} = 0$ for $j > n$;
(A2) $\sum_{j=1}^{n} a_{jn} = 1$ for all $n \geq 1$;
(A3) $\lim_{n\to\infty} a_{jn} = 0$ for all $j \geq 1$.

The sequence $\{x_n\}_{n=1}^{\infty}$ defined by

$$x_{n+1} = X(v_n), \quad \text{where } v_n = \sum_{j=1}^{n} a_{jn} x_j,$$

is called the Mann iterative process or, simply, the Mann iteration.

Definition 2.4: Lyapunov Exponent [25, p. 171]
Lyapunov states that we may take two points close to each other, like x_0 and $x_0 + \epsilon$. If the system is chaotic, then one would follow some trajectories. Still, the second point would diverge exponentially from the first point, which means both points would evolve in two different ways, and their separation of trajectories will increase in a bounded phase, as we may see in Fig. 1.

The distance between $\{x_0, x_0 + \epsilon\}$ and $\{f(x_0), f(x_0 + \epsilon)\}$ is given by:

$$d(x_0, x_0 + \epsilon) = d(f(x_0), f(x_0 + \epsilon)).$$

The exponential increment in separation is based on several iterations:

$$d(f(x_0), f(x_0 + \epsilon)) = e^{\lambda} d(f(x_0), f(x_0 + \epsilon)),$$

For the second iteration:

$$d(f^2(x_0), f^2(x_0 + \epsilon)) = e^{2\lambda} d(f(x_0), f(x_0 + \epsilon)),$$

$\vdots$

For the nth iteration:

$$d(f^n(x_0), f^n(x_0 + \epsilon)) = e^{n\lambda} d(f(x_0), f(x_0 + \epsilon)).$$

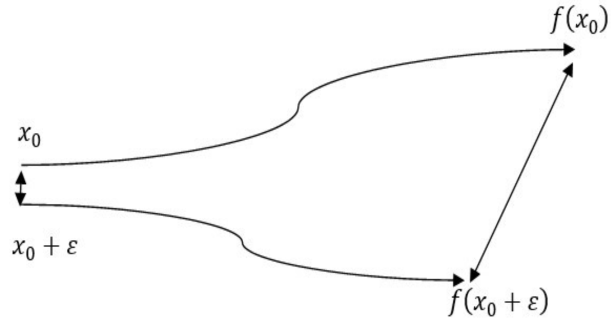

Fig. 1: Lyapunov exponent methodology

Image 1
We may write it as:

$$\lambda = \frac{1}{n} \ln\left(\frac{d(f^n(x_0), f(x_0 + \epsilon))}{\epsilon}\right)$$

Suppose the Lyapunov values are favorable for any system. In that case, a chaotic system is considered. If any system contains a maximal Lyapunov exponent, then it is believed it as the map system is better sensitive to dependence than a chaotic map.

Definition 2.5: Alternate System
Let us consider two different discrete dynamical systems D_1 and D_2 such as,

$$x_0 \xrightarrow{D_{k_0}} x_1 \xrightarrow{D_{k_1}} x_2 \xrightarrow{D_{k_2}} x_3, \ldots$$

Where x_0 denotes the initial condition value of the physical system, and k is a random or deterministic law that assigns values as 1 or 2 to each number of the sequences $\{0, 1, 2, 3, \ldots\}$, and $\{x_1, x_2, x_3, \ldots\}$ are the results or values of the variable x [2]. An alternate combination of the dynamics D_1 and D_2 are chaotic, but the one that results from a periodic change $D_1D_2D_1D_2D_1D_2 = (D_1D_2)$ is ordered in a clear sense and is depicted as “Chaos1 + Chaos2 = Order” [2]. Originally, the alternate system is called Parrondo’s Paradox [1]. We can use the above sequence in the following method:

$$D_{k_1k_2} : \begin{cases} x_n^2 + k_1, & \text{if } n \text{ is odd}, \\ x_n^2 + k_2, & \text{if } n \text{ is even}. \end{cases}$$

Where k is deterministic dynamical laws, and x is a real number.

Definition 2.6: Probability Density Function [26, p. 256]
Let f(x) be a probability function in the interval [a, b] then the

probability that the variate value x to lie within the interval [a, b] is given by

$$P(a \leq x \leq b) = \int_a^b f(x)\,dx$$

The function $f(x)$ has some important properties such as:

1) $f(x) \geq 0$ for all x.
2) The integral of the probability density function over its entire domain equals 1:
$$\int_a^b f(x)\,dx = 1.$$
3) For any value of x, the PDF would be 0 for a continuous random variable, i.e., $P(X = x) = 0$.

III. Proposed Work

We have proposed The Piecewise Logistic Map with a superior iteration method is defined as (Equ.-2).

Superior (Mann) iteration method (def. 2.3) has been used to transform the mathematical equation of PLM. Following this transformation, we applied alternate (def. 3.2) switching to the resulting equation.

IV. EXPERIMENTAL RESULTS

This section is divided into two parts. The first part presents the analysis of the stability, periodic, and instability behavior of SPLM by using a time series plot. The second part contains the exception in the behavior of SPLM for various numbers of segments (N) with parameters like β and μ. The piecewise logistic map (PLM), which is derived by iterating through the superior orbit (s.o.) using the Mann iteration method, is known as the superior piecewise logistic map (SPLM).

A. Behavior Analysis of SPLM via Time Series Plot

While chaotic maps are unpredictable due to sensitivity to initial conditions, mathematical techniques like nonlinear stability analysis allows studying their stability and periodicity by numerically simulating their behavior across parameters. The piecewise logistic map's nonlinear discontinuous form enables applying nonlinear analysis to examine its stability. The Time series of nonlinearity has also been explained by Mujiarto et. al. [27].

From Table I, we can see that $\forall x \in [0, 1]$ and $N = 4$

TABLE I: Behavior of PLM in S.O. at N = 4

β	Convergent behavior for μ	Periodic behavior for μ	Unstable behavior for μ
0.9	$0.0 < \mu \leq 0.77$	$0.77 < \mu \leq 0.98$	$0.98 < \mu \leq 2.34$
0.8	$0.0 < \mu \leq 0.84$	$0.84 < \mu \leq 1.05$	$1.05 < \mu \leq 2.55$
0.7	$0.0 < \mu \leq 0.91$	$0.91 < \mu \leq 1.17$	$1.17 < \mu \leq 2.86$
0.6	$0.0 < \mu \leq 1.04$	$1.04 < \mu \leq 1.31$	$1.31 < \mu \leq 3.26$
0.5	$0.0 < \mu \leq 1.20$	$1.20 < \mu \leq 1.47$	$1.47 < \mu \leq 3.82$
0.4	$0.0 < \mu \leq 1.43$	$1.43 < \mu \leq 1.66$	$1.66 < \mu \leq 4.67$
0.3	$0.0 < \mu \leq 1.80$	$1.80 < \mu \leq 2.02$	$2.02 < \mu \leq 6.08$
0.2	$0.0 < \mu \leq 2.59$	$2.59 < \mu \leq 2.81$	$2.81 < \mu \leq 8.91$
0.1	$0.0 < \mu \leq 4.84$	$4.84 < \mu \leq 5.29$	$5.29 < \mu \leq 17.39$

at $\beta = 0.9$; if we put $0 \leq \mu \leq 0.77$, then the trajectory of SPLM converges to a fixed point, and this convergent behavior is represented by (Fig. 2). After increasing the μ value from 1.21 to 1.47 (i.e., $1.20 < \mu \leq 1.47$) for $\beta = 0.5$, its behavior changes from convergent to periodic (see Fig. 3). Similarly, if we increase the μ value from 5.30 to 17.39 for $\beta = 0.1$, its behavior changes from periodicity to instability, as illustrated in Fig. 4.

From Table IV, we can see that $\forall x \in [0, 1]$ and $N = 5$

TABLE II: Behavior of PLM in S.O. at N = 5

β	Convergent behavior for μ	Periodic behavior for μ	Unstable behavior for μ
0.9	$0.0 < \mu \leq 0.60$	$0.60 < \mu \leq 0.77$	$0.77 < \mu \leq 1.10$
0.8	$0.0 < \mu \leq 0.66$	$0.66 < \mu \leq 0.85$	$0.85 < \mu \leq 1.21$
0.7	$0.0 < \mu \leq 0.74$	$0.74 < \mu \leq 0.93$	$0.93 < \mu \leq 1.37$
0.6	$0.0 < \mu \leq 0.83$	$0.83 < \mu \leq 1.06$	$1.06 < \mu \leq 1.60$
0.5	$0.0 < \mu \leq 0.95$	$0.95 < \mu \leq 1.21$	$1.21 < \mu \leq 1.97$
0.4	$0.0 < \mu \leq 1.10$	$1.10 < \mu \leq 1.41$	$1.41 < \mu \leq 2.58$
0.3	$0.0 < \mu \leq 1.46$	$1.46 < \mu \leq 1.68$	$1.68 < \mu \leq 3.53$
0.2	$0.0 < \mu \leq 2.10$	$2.10 < \mu \leq 2.26$	$2.26 < \mu \leq 5.51$
0.1	$0.0 < \mu \leq 4.02$	$4.02 < \mu \leq 4.23$	$4.23 < \mu \leq 10.76$

at $\beta = 0.9$, if we put $0 \leq \mu \leq 0.62$, then the trajectory of SPLM converges to a fixed. After decreasing the β value from 0.9 to 0.5 and increasing the μ value from 0.95 till 1.24 (i.e., $0.95 \leq \mu \leq 1.24$), then its behavior is three-step periodic. Again, if decreasing the β value from 0.5 to 0.1 and increasing the μ value from 2.24 to 10.76, then its behavior is unstable.

From Table III, we can see that $\forall x \in [0, 1]$ and $N = 10$ at

TABLE III: Behavior of PLM in S.O. at N = 10

β	Convergent behavior for μ	Periodic behavior for μ	Unstable behavior for μ
0.9	$0.0 < \mu \leq 0.30$	$0.30 < \mu \leq 0.38$	$0.38 < \mu \leq 0.92$
0.8	$0.0 < \mu \leq 0.32$	$0.32 < \mu \leq 0.42$	$0.42 < \mu \leq 1.03$
0.7	$0.0 < \mu \leq 0.37$	$0.37 < \mu \leq 0.49$	$0.49 < \mu \leq 1.14$
0.6	$0.0 < \mu \leq 0.41$	$0.41 < \mu \leq 0.52$	$0.52 < \mu \leq 1.34$
0.5	$0.0 < \mu \leq 0.47$	$0.47 < \mu \leq 0.59$	$0.59 < \mu \leq 1.53$
0.4	$0.0 < \mu \leq 0.57$	$0.57 < \mu \leq 0.66$	$0.66 < \mu \leq 1.86$
0.3	$0.0 < \mu \leq 0.74$	$0.74 < \mu \leq 0.80$	$0.80 < \mu \leq 2.43$
0.2	$0.0 < \mu \leq 1.06$	$1.06 < \mu \leq 1.13$	$1.13 < \mu \leq 3.56$
0.1	$0.0 < \mu \leq 1.98$	$1.98 < \mu \leq 2.12$	$2.12 < \mu \leq 6.96$

$\beta = 0.9$, the convergent range exists between the range of μ is $0 \leq \mu \leq 0.31$ (Fig. 8), periodic behavior (Fig. 9) range of μ is $0.47 \leq \mu \leq 0.58$ with the β value is 0.5, and unstable range is $0.46 \leq \mu \leq 0.48$ with β value is 0.3 (Fig. 10).

By following the explanation of Table I, II, and II, it can be said that for Table IV, i.e., $\forall x \in [0, 1]$ and $N = 16$ at $\beta = 0.9$, if we put $0 \leq \mu \leq 0.19$, then the SPLM represents the convergent behavior which is characterized by (Fig. 5). It shows periodic behavior of $N = 16$ at $\beta = 0.5$ if μ value is from 0.30 to 0.36 (i.e., $0.30 \leq \mu \leq 0.36$), which is represented by (Fig. 6). Again, if we increase the μ value from 1.35 to 4.35, then its behavior changes from periodicity to instability, which can be seen in (Fig. 7).

From Table III, we may say that $\forall x \in [0, 1]$ and $N = 32$ at $\beta = 0.9$; if we put $0 < \mu \leq 0.09$, then the SPLM represents the convergent behavior (Fig. 8). It shows periodic behavior at $N = 32$ and $\beta = 0.5$ if the μ value is from 0.16 till 0.18 (i.e., $0.15 < \mu \leq 0.18$ (Fig. 9)). Again, if we increase the μ value from 0.68 to 2.17 at $\beta = 0.1$, then its behavior changes from periodicity to instability (Fig. 10).

From Table IV, it is visible that for all $x \in [0, 1]$ and $N = 64$ at $\beta = 0.9$, the convergent range exists between the range of $0 < \mu \leq 0.04$ (see Fig. 11), periodic behavior (see Fig. 12) occurs in the range of $0.07 \leq \mu \leq 0.09$ with

$$F_c : f(x_n, \mu) = x_{n+1} = \begin{cases} N^2\mu\beta(x_n - \frac{i-1}{N})(\frac{i}{N} - x_n) + (1-\beta)(x_n - \frac{i-1}{N}), & \text{for } \frac{i-1}{N} < x_n < \frac{i}{N} \\ 1 - N^2\mu\beta(x_n - \frac{i-1}{N})(\frac{i}{N} - x_n) + (1-\beta)(x_n - \frac{i-1}{N}), & \text{for } \frac{i}{N} < x_n < \frac{i+1}{N} \\ (x_n + \frac{1}{100N}) + (1-\beta)x_n, & \text{for } x_n = 0, \frac{1}{N}, \frac{2}{N}, \frac{3}{N}, ..., \frac{N-1}{N} \\ (x_n - \frac{1}{100N}) - (1-\beta)x_n, & \text{for } x_n = 1 \end{cases} \tag{2}$$

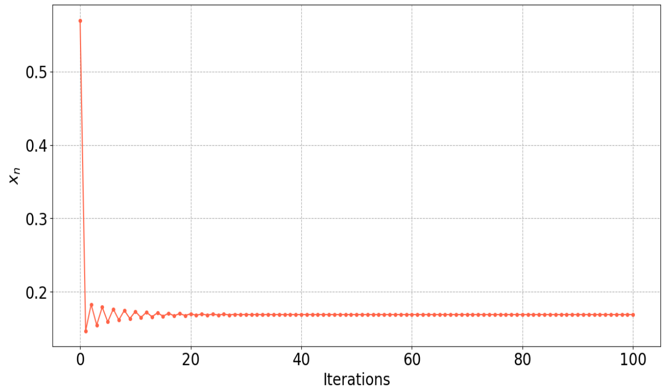

Fig. 2: Convergent time series plot for N = 4, $\beta = 0.9$, and $\mu = 0.77$

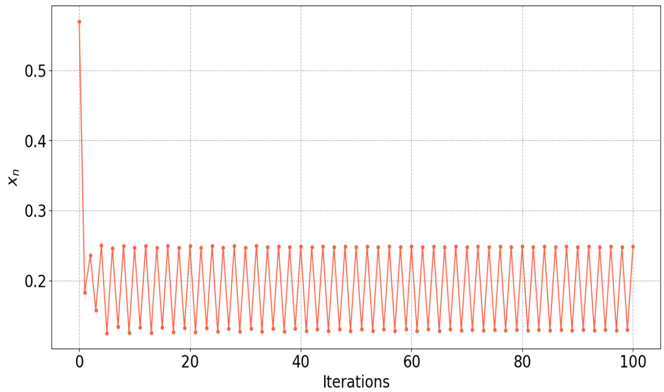

Fig. 3: Periodic time series plot for N = 4, $\beta = 0.5$, and $\mu = 1.47$

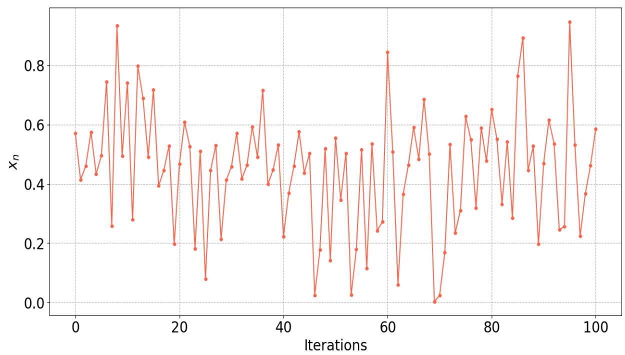

Fig. 4: Unstable time series plot for N = 4, $\beta = 0.1$, and $\mu = 17.39$

$\beta = 0.5$, and the unstable range is $0.36 \le \mu \le 1.08$ with $\beta = 0.1$. Fig. 13 is the graphical representation of erratic behavior.

B. Exception in the Behavior of SPLM

The current study has used the N (number of segments) values as 4, 16, 32, and 64 iterated using the superior iteration

TABLE IV: Behavior of PLM in S.O. at N = 16

β	**Convergent behavior for μ**	**Periodic behavior for μ**	**Unstable behavior for μ**
0.9	$0.0 < \mu \le 0.19$	$0.19 < \mu \le 0.24$	$0.24 < \mu \le 0.81$
0.8	$0.0 < \mu \le 0.21$	$0.21 < \mu \le 0.26$	$0.26 < \mu \le 0.63$
0.7	$0.0 < \mu \le 0.23$	$0.23 < \mu \le 0.29$	$0.29 < \mu \le 0.71$
0.6	$0.0 < \mu \le 0.26$	$0.26 < \mu \le 0.32$	$0.32 < \mu \le 0.81$
0.5	$0.0 < \mu \le 0.29$	$0.29 < \mu \le 0.33$	$0.36 < \mu \le 0.95$
0.4	$0.0 < \mu \le 0.36$	$0.36 < \mu \le 0.41$	$0.41 < \mu \le 1.16$
0.3	$0.0 < \mu \le 0.46$	$0.46 < \mu \le 0.50$	$0.50 < \mu \le 1.52$
0.2	$0.0 < \mu \le 0.64$	$0.64 < \mu \le 0.70$	$0.70 < \mu \le 2.23$
0.1	$0.0 < \mu \le 1.26$	$1.26 < \mu \le 1.34$	$1.34 < \mu \le 4.35$

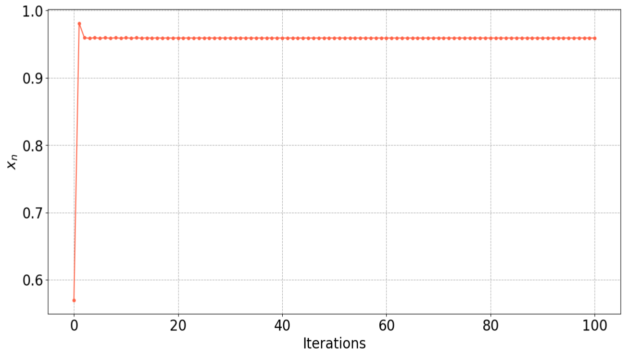

Fig. 5: Convergent time series plot for N = 16, $\beta = 0.9$, and $\mu = 0.19$

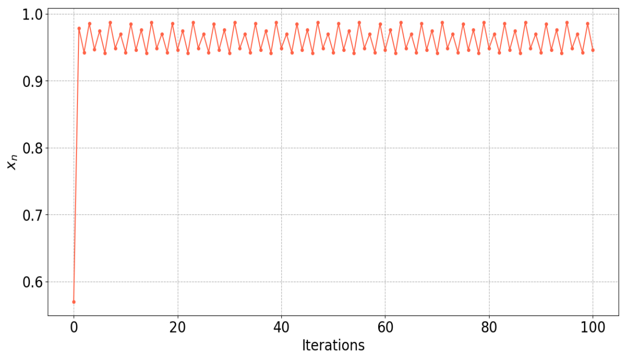

Fig. 6: Periodic time series plot for N = 16, $\beta = 0.5$, and $\mu = 0.33$

TABLE V: Behavior of PLM in S.O. at N = 32

β	**Convergent behavior for μ**	**Periodic behavior for μ**	**Unstable behavior for μ**
0.9	$0.0 < \mu \le 0.09$	$0.09 < \mu \le 0.13$	$0.13 < \mu \le 0.39$
0.8	$0.0 < \mu \le 0.10$	$0.10 < \mu \le 0.13$	$0.13 < \mu \le 0.31$
0.7	$0.0 < \mu \le 0.11$	$0.11 < \mu \le 0.14$	$0.14 < \mu \le 0.35$
0.6	$0.0 < \mu \le 0.12$	$0.12 < \mu \le 0.16$	$0.16 < \mu \le 0.40$
0.5	$0.0 < \mu \le 0.15$	$0.15 < \mu \le 0.18$	$0.18 < \mu \le 0.47$
0.4	$0.0 < \mu \le 0.18$	$0.18 < \mu \le 0.20$	$0.20 < \mu \le 0.58$
0.3	$0.0 < \mu \le 0.23$	$0.23 < \mu \le 0.25$	$0.25 < \mu \le 0.76$
0.2	$0.0 < \mu \le 0.33$	$0.33 < \mu \le 0.35$	$0.35 < \mu \le 1.11$
0.1	$0.0 < \mu \le 0.63$	$0.63 < \mu \le 0.67$	$0.67 < \mu \le 2.17$

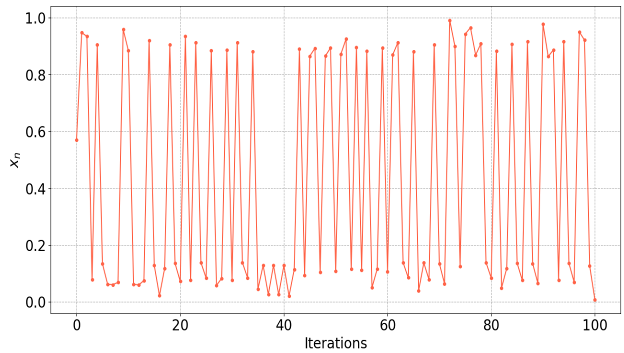

Fig. 7: Unstable time series plot for N = 16, $\beta = 0.1$, and $\mu = 4.35$

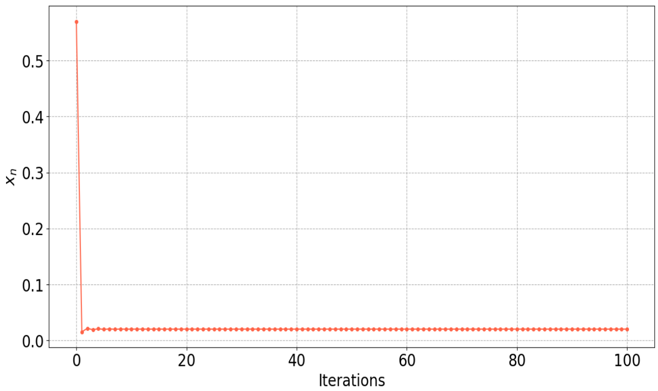

Fig. 8: Convergent time series plot for N = 32, $\beta = 0.9$, and $\mu = 0.09$

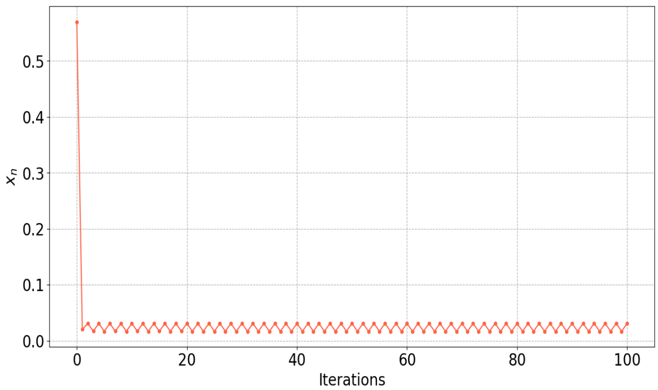

Fig. 9: Periodic time series plot for N = 32, $\beta = 0.5$, and $\mu = 0.18$

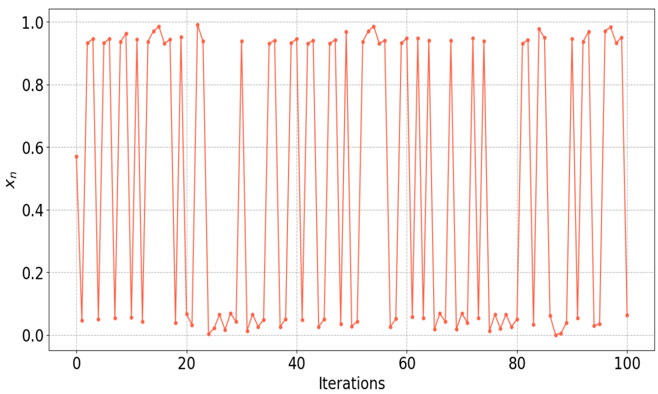

Fig. 10: Unstable time series plot for N = 32, $\beta = 0.1$, and $\mu = 2.17$

TABLE VI: Behavior of PLM in S.O. at N = 64

β	**Convergent behavior for μ**	**Periodic behavior for μ**	**Unstable behavior for μ**
0.9	$0.0 < \mu \leq 0.04$	$0.04 < \mu \leq 0.06$	$0.06 < \mu \leq 0.24$
0.8	$0.0 < \mu \leq 0.05$	$\mu = 0.06$	$0.06 < \mu \leq 0.15$
0.7	$0.0 < \mu \leq 0.05$	$0.05 < \mu \leq 0.07$	$0.07 < \mu \leq 0.17$
0.6	$0.0 < \mu \leq 0.06$	$0.06 < \mu \leq 0.08$	$0.08 < \mu \leq 0.20$
0.5	$0.0 < \mu \leq 0.07$	$0.07 < \mu \leq 0.09$	$0.09 < \mu \leq 0.23$
0.4	$0.0 < \mu \leq 0.09$	$\mu = 0.10$	$0.10 < \mu \leq 0.29$
0.3	$0.0 < \mu \leq 0.11$	$\mu = 0.12$	$0.12 < \mu \leq 0.38$
0.2	$0.06 < \mu \leq 0.16$	$\mu = 0.17$	$0.17 < \mu \leq 0.55$
0.1	$0.06 < \mu \leq 0.31$	$0.31 < \mu \leq 0.36$	$0.36 < \mu \leq 1.08$

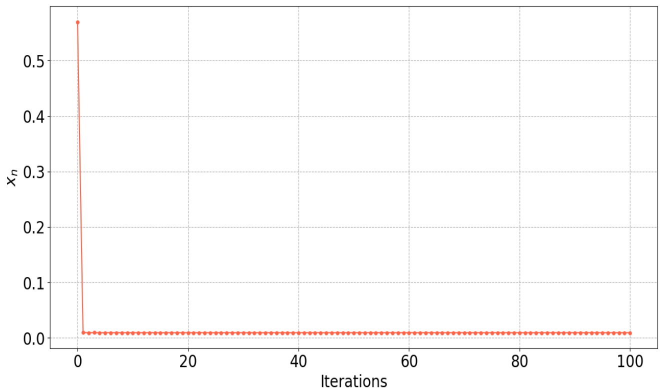

Fig. 11: Convergent time series plot for N = 64, $\beta = 0.9$, and $\mu = 0.04$

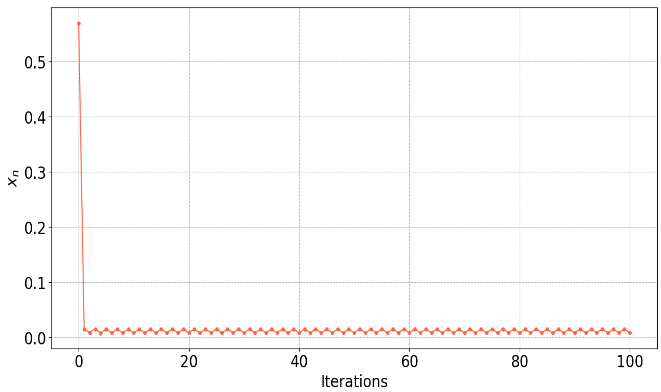

Fig. 12: Periodic time series plot for N = 64, $\beta = 0.5$, and $\mu = 0.09$

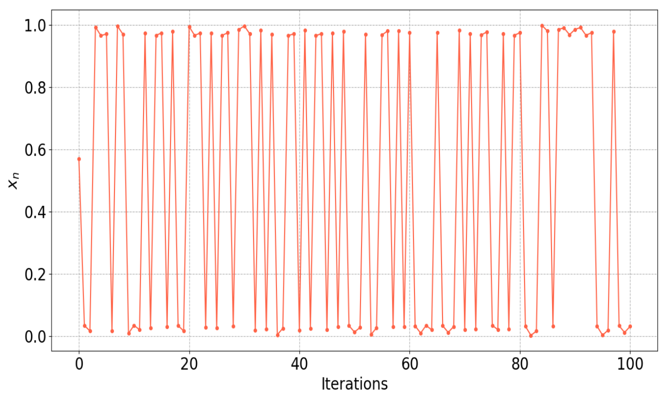

Fig. 13: Unstable time series plot for N = 64, $\beta = 0.1$, and $\mu = 1.08$

method for all N values and $x \in [0, 1]$ at $0 < \beta \leq 0.9$. In this entire calculation, many exceptions stand out (Table VII); for example, when $N = 4$, $\beta = 0.9$, the instability range is from 0.99 to 2.34, but the μ values like $1.04, 1.10, 1.14, 1.20$ to $1.24, 1.74$ to 1.85, and 2.24 exhibiting periodic behavior, and 1.58 to 1.73 exhibiting convergent behavior. For $N = 4$, $\beta = 0.8$, the instability range is from 1.08 to 2.55, but among this range, the μ values like 1.30 to $1.34, 1.44, 1.52, 1.91$ to $2.05, 2.10, 2.32$, and 2.46 represent the periodic behavior, and 1.72 to 1.90 represent convergent behavior. Similarly, if we set $N = 16, 32$, and 64 for all $\beta \in [0.1, 0.9]$ and $x \in [0, 1]$, then convergent and periodic behavior falls at many points among the range of instability of μ.

TABLE VII: Exception in behavior of SPLM with all of segments

S. No	N = 4	N = 16	N = 32	N = 64
1	0.308	0.221	0.111	0.227
2	0.883	0.978	0.491	0.210
3	2.030	0.642	0.320	0.185
4	3.922	0.439	0.220	0.119
5	0.176	0.348	0.138	
6	2.561	0.273	0.119	
7	1.750	0.234	0.101	
8	0.333	0.199	0.090	
9	0.122	0.178		
10		0.159		
11		0.142		
12		0.132		
13		0.123		
14		0.109		
15		0.103		
16		0.094		
Total				
Gaps	9	16	8	3

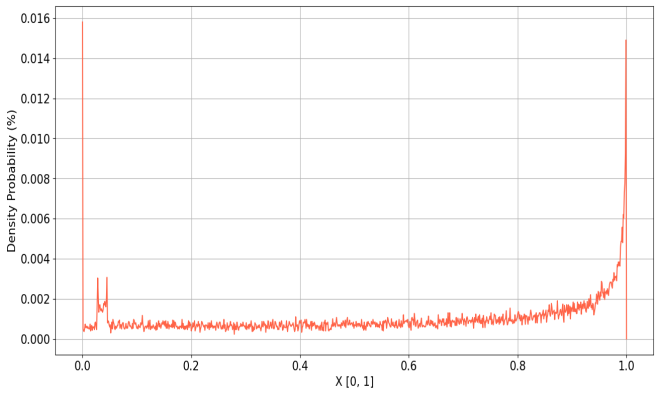

Fig. 14: SPLM density probability distribution at N = 32, $\beta = 0.1$, and $\mu = 39.45$

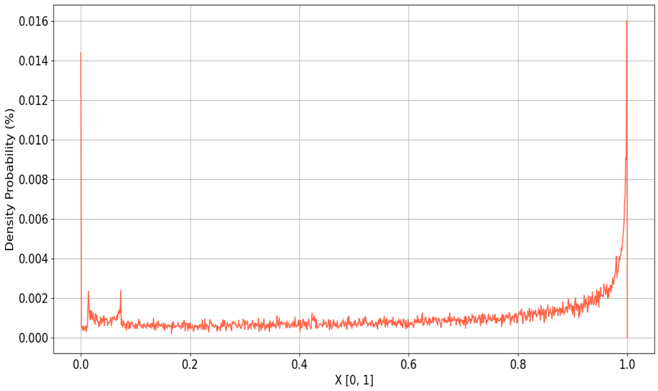

Fig. 15: SPLM density probability distribution at N = 64, $\beta = 0.1$, and $\mu = 39.73$

V. THE DENSITY PROBABILITY DISTRIBUTION OF SPLM

There are three different parameters in SPLM, i.e., N is used for several segments in the SPLM map, β (beta) is used for superior iteration, and μ (mu) is used for the growth rate. Sometimes, this μ is denoted as r, known as biotic potential. The probability distribution (you may see Def. 2.6) illustrates equal results in the given range, and here, the uniformity of the state value of SPLM will be evaluated with the help of the above three different parameters (N, β, μ). If $\beta = 1$ is used in Equ. 1, the equation will work like a piecewise logistic map, and the iteration will become Picard. Still, we should use superior iteration on this piecewise logistic map for our objective. So, the above method has been used to analyze the density probability distribution in SPLM.

When the Picard iteration method is used, its behavior shows the uniform distribution for any N value; please refer to [24] for more details. Let us consider Table III for $N = 32$ at $\beta = 0.1$ and $\mu = 39.45$, and Table IV for $N = 64$ at $\beta = 0.1$ and $\mu = 39.73$, which also show uniform distribution (see Fig. 14, Fig. 15). The SPLM is iterated with $N = 32$ and $N = 64$ over 100,000 iterations, with the interval $[0, 1]$ being partitioned into 1250 subintervals. The density distribution is created by calculating the likelihood that state values will occur within each sub-interval. The distribution that results is consistent over a range of N values and closely matches the traditional piecewise logistic map.

VI. LYAPUNOV EXPONENTS PARAMETERIZED DIAGRAM OF SPLM

There are two ways to characterize chaotic orbits and non-chaotic orbits: 1) (a) Box counting direction, (b) correlation dimension, and 2) Lyapunov exponent. The box-counting direction and correlation dimension are used to quantify how distributed the points of the orbits are; they do not quantify precisely the sensitive dependence on the initial condition, and this quantification is used in both continuous time dynamical systems and discrete-time dynamical systems for more details [28][29].

When we keep $N = 4$ and $\beta = 0.1$ (Table I), the logarithmic transformation of the Lyapunov exponent increased to $20.0\,\mu$ (Fig. 16). It attains state values ranging from 0 to 0.68, demonstrating sensitivity to initial conditions; yet, its results also reveal a mixture of stable (trending negative), neutral (values at 0), and chaotic (unpredictable) states.

After increasing the value of N from 4 to 5 at $\beta = 0.1$ (Table II), the logarithmic transformation reached its highest value of 1.11 with $\mu = 36.32$, and the intensity of the chaotic numbers increased compared to $N = 4$ (Fig. 17). Similarly, when the value of N was further increased from 5 to 10 at $\beta = 0.1$ (Table III), the logarithmic transformation improved to 2.04, and the intensity of chaotic numbers increased compared to $N = 5$ (Fig. 18).

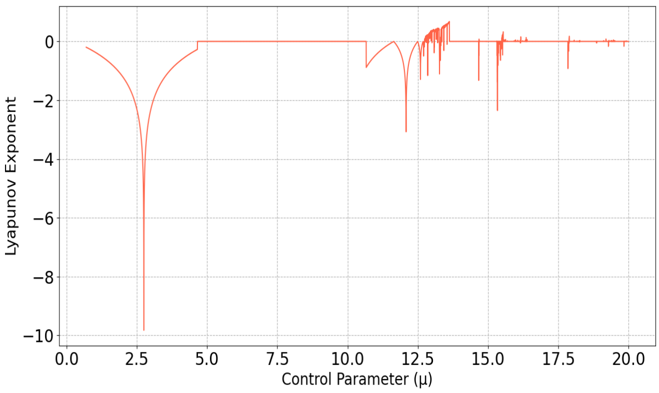

Fig. 16: Lyapunov exponent for N = 4, $\beta = 0.1$, and $\mu = 20$

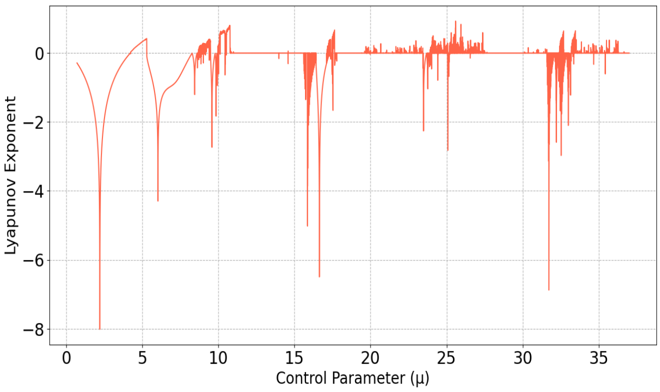

Fig. 17: Lyapunov exponent for N = 5, $\beta = 0.1$, and $\mu = 36.32$

When we increase the N value from 10 to $N = 16$ at $\beta = 0.1$ (Table IV), the logarithmic transformation of the Lyapunov exponent increased from 0.68 to 2.84 (Fig. 17) and its sensitivity to initial conditions has increased but with the mixture of less stable, less neutral, and highly chaotic states. The same thing happened as the intensity increased. The logarithmic transformation remains the same when taking $N = 32$ for $\beta = 0.1$ (Table V). Here, the state value increased from 2.84 to more than 3.84 (Fig. 18), and the intensity of the chaotic number series increased compared to all previous segments ($N = 4$, and 16).

When $N = 64$ and $\beta = 0.1$ (Table VI), the logarithmic transformation goes up to 39.78 μ by containing the property of sensitivity to initial conditions with higher sensitivity. Here, the state value increased from 3.84 to 4.57 (Fig. 19). Intensity was achieved at its highest (for comparative analysis, you may refer to [30][31][32], including all the values of the tables.

VII. PARAMETERIZED TIME SERIES PLOT-BASED BIFURCATION DIAGRAM OF SPLM

In the bifurcation diagram of the PLM with N and β values, simulations has been performed. With the help of the given tables, it is known that the logarithmic transformation limit r varies by increasing N values and decreasing β values. Bifurcation diagrams based on different N and β parameters have been provided. The common problem in all basic maps is the periodic window glitch, which presents the exception for the range of chaotic values.

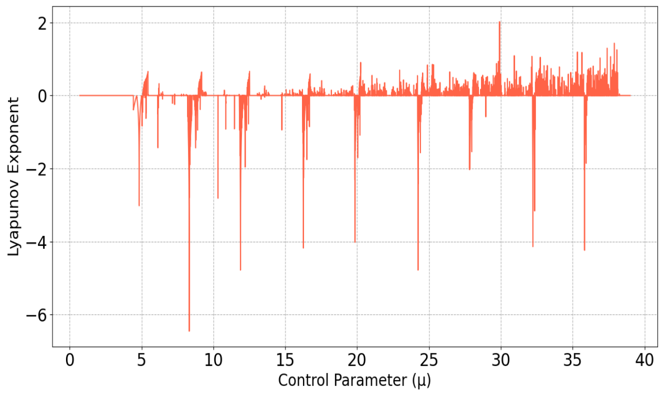

Fig. 18: Lyapunov exponent for N = 10, $\beta = 0.1$, and $\mu = 38.25$

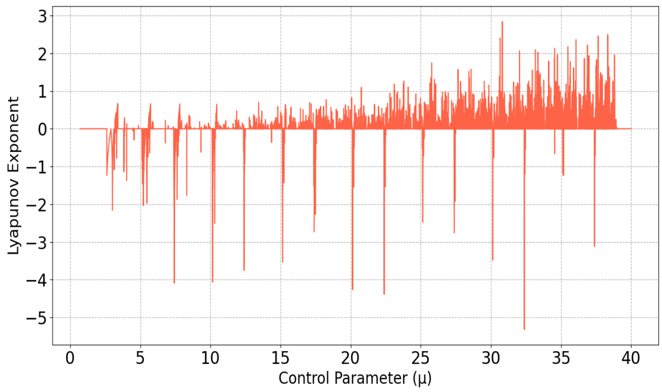

Fig. 19: Lyapunov exponent for N = 16, $\beta = 0.1$, and $\mu = 38.93$

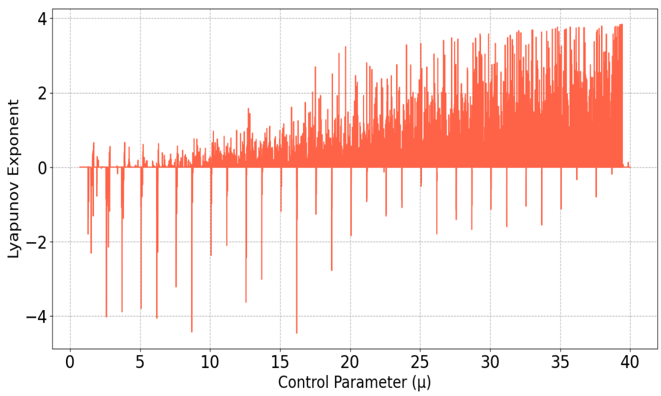

Fig. 20: Lyapunov exponent for N = 32, $\beta = 0.1$, and $\mu = 39.52$

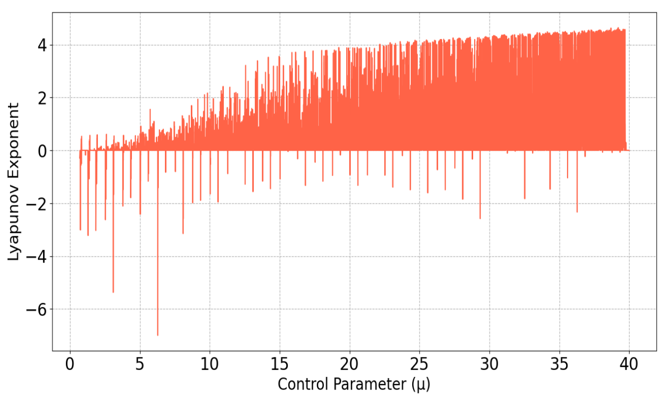

Fig. 21: Lyapunov exponent for N = 64, $\beta = 0.1$, and $\mu = 39.82$

The PLM removed this problem after increasing the N values. However, the logarithmic transformation value is still as it is in the logistic map (for more instances), i.e., $\mu = 4$ [35]. But when we applied superior iteration on this PLM, the logarithmic transformation increased till more or less $\mu = 40$. It is found that as the number of segments (N) and decrease the values of β, the chaotic limit increases, and the convergence limit decreases. Possible long-term state values of the PLM are depicted on the vertical axis, with control parameters on the horizontal axis.

PLM, an enhanced version of the logistic map, exhibits bifurcation patterns similar to the logistic map, specifically, flip (periodic-doubling) based bifurcation [33]. A chaotic regime occurs when bifurcation cascades due to an increment of control parameters. After applying the superior iteration on PLM, its logarithmic transformation increases. Whenever we increase the N value and decrease the β value, its convergent area decreases, and the chaotic region increments. This superior iteration method not only increases the chaotic region but also removes the earlier window glitch in the logistics map and provides one of the best chaotic maps, which contains the highest chaotic range.

When we consider $N = 4$ and $\beta = 0.1$ in the SPLM function defined in (def. 3.1), then the range of its logarithmic transformation goes up to 35.35 μ, and we have a count that there are nine window glitches in total (Fig. 24) which are represented as a numeric form in the upper side of images. After incrementing the N value from 4 to 16, 32, and then 64, their transformation ranges are 38.86 (Fig. 25), 39.43 (Fig. 26), and 39.72 (Fig. 27), respectively. There are 9, 16, 8, and 4 window glitches. We can see that at $N = 64$, the logarithmic transformation range will be approximately 40 μ (Fig. 27). Still, if we talk about the pure chaotic range, which has the highest intensity of chaotic values, it is from 20 μ to 39.72 (Fig. 24). The length of all these window glitches is shown in Table V.

VIII. Alternate Superior Orbit with Different μ

The alternate system [1] represents a variant of Parrondo's paradox, also known as the switching strategy. In Parrondo's paradox, combining two distinct complex systems may yield a more straightforward system, such as *chaos*^{1} + *chaos*^{2}, resulting in order, or two simple systems combining to form a complex system, like *Order*^{1} + *Order*^{2}, leading to chaos. We applied this methodology to SPLM, utilizing two constants, μ, and β, and iterating through the process.

Found order values in the periodic form by taking the two chaotic values. Fig. 20 shows that the system converts to the periodic form when we take two different μ from the chaotic range and alternately iterate $\mu_1 = 12.5056$ and $\mu_2 = 17.3900$ at $N = 4$, $\beta = 0.1$. Similarly, when we set $N = 16$, 32, and 64 with $[3.9960, 4.3500]$ μ (Fig. 21), $[1.5994, 2.4100]$ μ (Fig. 22) and $[0.3770, 1.1200]$ μ (Fig. 23) represent periodic convergent.

IX. NIST (Randomness) Test

Statistical randomness is a fundamental requirement for various applications, especially in cryptography and simulation. The NIST SP 800-22 test suite [19][14] is widely regarded as a standard tool for assessing the randomness of binary sequences. This test suite includes 15 distinct statistical tests of which we have included only 13 that designed to detect deviations from random behavior. The results of these tests help determine whether a sequence exhibits the properties of randomness.

Although the NIST SP 800-22 test suite is a robust tool for randomness evaluation[34], it does not guarantee absolute statistical strength. New tests may reveal weaknesses in the generator under examination. Therefore, comprehensive evaluation using multiple statistical approaches remains crucial for validating randomness.

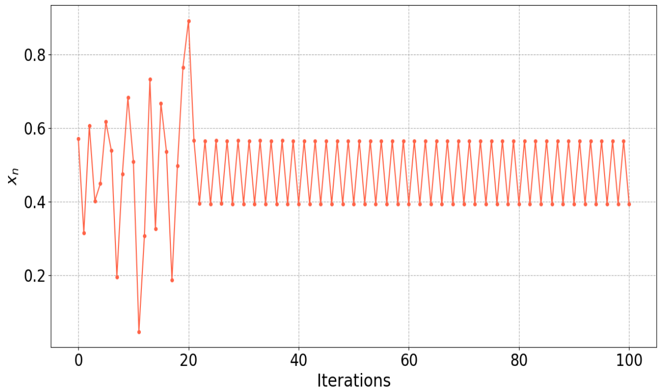

Fig. 22: SPLM alternate time series plot for N = 4, $\beta = 0.1$, $\mu_1 = 12.5056$, and $\mu_2 = 17.3900$

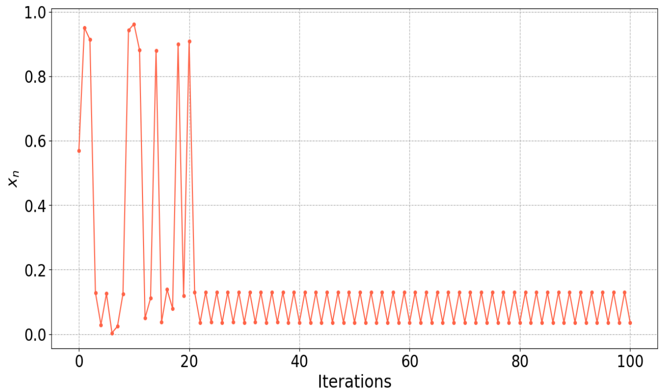

Fig. 23: SPLM alternate time series plot for N = 16, $\beta = 0.1$, $\mu_1 = 3.9960$, and $\mu_2 = 4.3500$

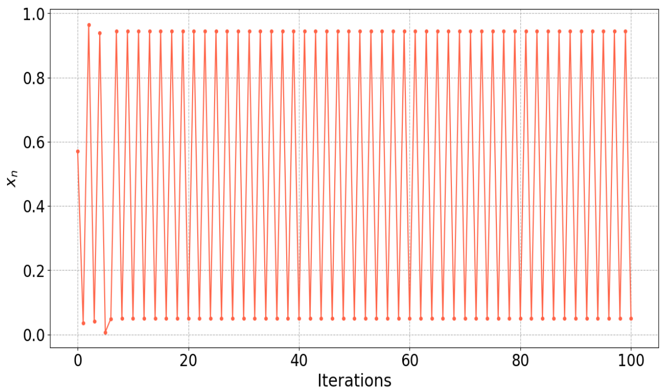

Fig. 24: SPLM alternate time series plot for N = 32, $\beta = 0.1$, $\mu_1 = 1.5994$, and $\mu_2 = 2.4100$

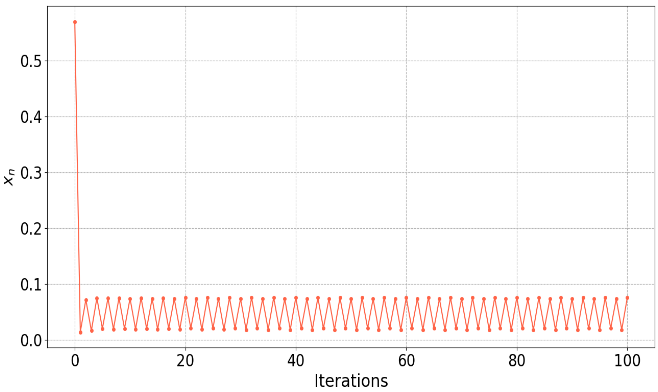

Fig. 25: SPLM alternate time series plot for N = 64, $\beta = 0.1$, $\mu_1 = 0.3770$, and $\mu_2 = 1.2000$

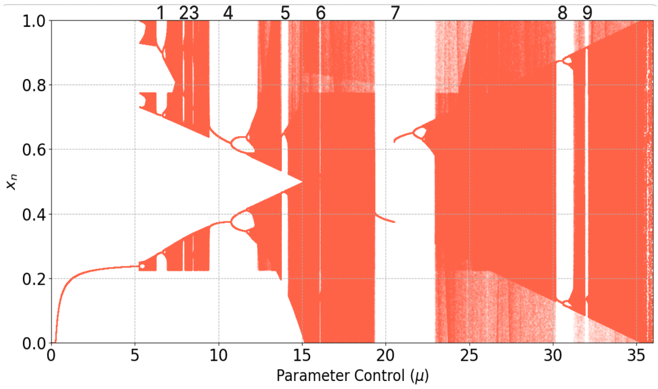

Fig. 26: SPLM bifurcation for N = 4, $\beta = 0.1$, and $\mu = 35.35$

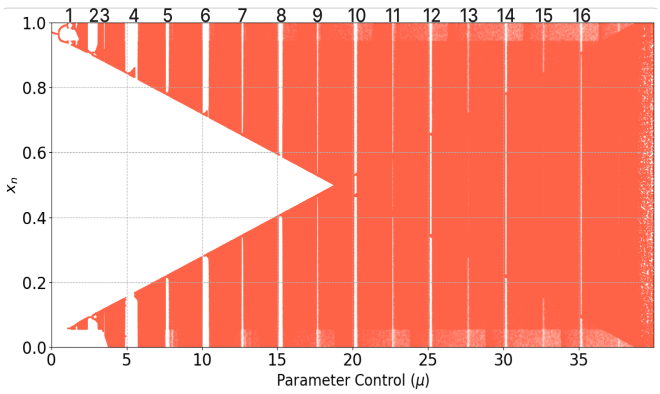

Fig. 27: SPLM bifurcation for N = 16, $\beta = 0.1$, and $\mu = 38.86$

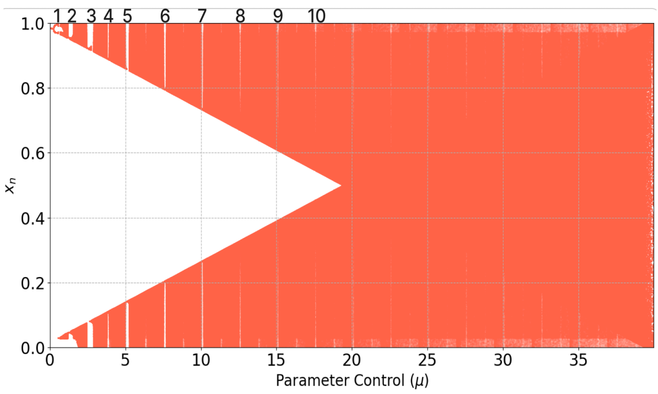

Fig. 28: SPLM bifurcation for N = 32, $\beta = 0.1$, and $\mu = 39.43$

The results of the NIST test (Table VIII) evaluation highlight the strengths and weaknesses of the random

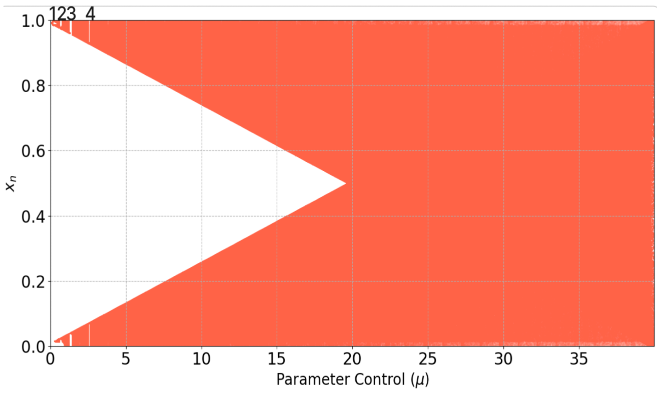

Fig. 29: SPLM bifurcation for N = 64, $\beta = 0.1$, and $\mu = 39.72$

TABLE VIII: Results of NIST SP 800-22 Test Suite

Test Name	Proportion	P-Value	Result
Frequency	10/10	0.534146	Pass
BlockFrequency	10/10	0.911413	Pass
CumulativeSums	10/10	0.534146	Pass
Runs	10/10	0.213309	Pass
LongestRun	10/10	0.350485	Pass
Rank	10/10	0.122325	Pass
FFT	10/10	0.350485	Pass
NonOverlappingTemplate	10/10	0.911413	Pass
Universal	10/10	0.000000	Fail
ApproximateEntropy	3/10	0.000000	Fail
Serial	10/10	0.911413	Pass
Serial	10/10	0.122325	Pass
LinearComplexity	10/10	0.739918	Pass

number generator through the chaotic maps [35]. Out of 13 tests, the system successfully passed 11, achieving perfect 10/10 proportions and maintaining p-values above 0.01. Notable strengths were observed in the Frequency, Block Frequency, Runs, and Linear Complexity tests, which reflect the generator's capability to produce sequences with solid fundamental randomness.

Despite these positive outcomes, the generator failed two critical tests: the Universal test and the Approximate Entropy test. Both tests yielded p-values of 0.000000, with the Approximate Entropy test showing a particularly low proportion of 3/10. These results indicate significant deficiencies in the sequence's entropy, raising concerns about potential predictability.

The Serial test was conducted twice and passed consistently, underscoring robust sequential randomness. While most of the tests displayed high p-values ranging between 0.122325 and 0.911413, the two failed tests reveal vulnerabilities that might render the generator unsuitable for cryptographic uses without addressing these shortcomings.

X. Image Encryption with the Proposed SPLM

We successfully implemented image encryption by utilizing our proposed SPLM (as detailed in Algorithm 1) on four standard images sourced from the SIPI database (refer to Table IX for more information). The results of the encryption are presented in Figures 30-33, which illustrate both the original and encrypted versions of the images. The procedures for encryption and decryption are comprehensively outlined in Algorithms 2-4, providing a clear understanding of the steps

(a) Original image (b) Encrypted image

Fig. 30: Original and encrypted images of peppers

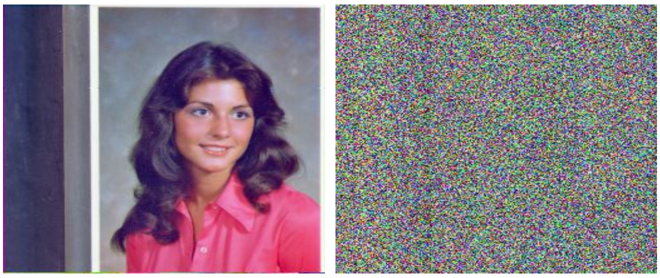

(a) Original image (b) Encrypted image

Fig. 31: Original and encrypted images of female

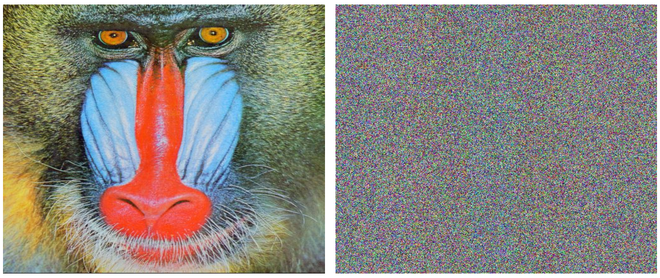

(a) Original image (b) Encrypted image

Fig. 32: Original and encrypted images of Mandrill

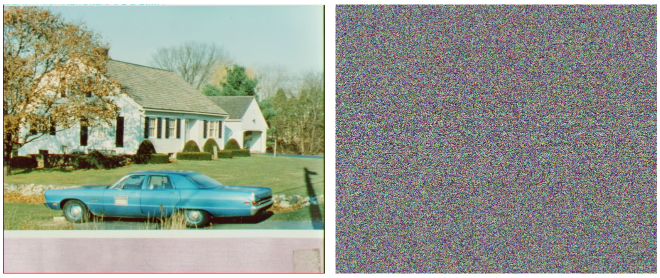

(a) Original image (b) Encrypted image

Fig. 33: Original and encrypted images of house

involved in these processes. When compared to conventional encryption methods, the SPLM technique showcases notable advancements in terms of security, offering enhanced protection for image data.

TABLE IX: Table of Image Data

Name of Image	Dimension	Database
Peppers.tiff	512*512	SIPI
Female.tiff	256*256	SIPI
Mandrill.tiff (a.k.a. Baboon)	512*512	SIPI
House.tiff	512*512	SIPI

Algorithm 1 Superior Piecewise Logistic Map (SPLM)

Require: x, N, μ, β
Ensure: Updated x

if $x \in \{i/N \mid i = 0, 1, \ldots, N\}$ **then**
  if $x == 0$ or $x == 1$ **then**
    return $x \pm (1/100N) + (1-\beta)x$
  else
    return $x + (1/100N) + (1-\beta)x$
  end if
end if
for $i = 0$ to $N-1$ **do**
  $lower\_bound \leftarrow i/N$
  $upper\_bound \leftarrow (i+1)/N$
  if $lower\_bound < x < upper\_bound$ **then**
    if $i\%2 == 0$ **then**
      return $N^2\mu\beta(x - lower\_bound)(upper\_bound - x) + (1-\beta)(x - lower\_bound)$
    else
      return $1 - N^2\mu\beta(x - lower\_bound)(upper\_bound - x) + (1-\beta)(x - lower\_bound)$
    end if
  end if
end for
return x =0

Algorithm 2 Create Key

Require: $width$, $height$, $seed$, $channels$
Ensure: Key matrix

Initialize parameters: $N \leftarrow 512$, $\mu \leftarrow 38.82$, $\beta \leftarrow 0.1$
Initialize array x of size $width \times height \times channels$
$x[0] \leftarrow seed$
for $i = 1$ to $width \times height \times channels - 1$ **do**
  $x[i] \leftarrow SPLM(x[i-1], N, \mu, \beta)$
end for
return $((x - min(x)) \times 256/(max(x) - min(x)))$ =0

Algorithm 3 Create Permutation

Require: $length$, $seed$
Ensure: Permutation sequence

Initialize parameters: $N \leftarrow 512$, $\mu \leftarrow 38.82$, $\beta \leftarrow 0.1$
Initialize array x of size $length$
$x[0] \leftarrow seed$
for $i = 1$ to $length - 1$ **do**
  $x[i] \leftarrow SPLM(x[i-1], N, \mu, \beta)$
end for
return $argsort(x)$ =0

Algorithm 4 Encrypt Image

Require: $image\_path$, $seed$
Ensure: Encrypted image, permutation, key

Load $image$ from $image\_path$
Get $height$, $width$, $channels$ of $image$
$key \leftarrow$ Create Key($width$, $height$, $seed$, $channels$)
$permutation \leftarrow$ Create Permutation($height$, $seed$)
Apply $permutation$ to rows of $image$
$encrypted\_image \leftarrow image \oplus key$
return $encrypted\_image$, $permutation$, key =0

Algorithm 5 Decrypt Image

Require: $encrypted\_image$, $permutation$, key
Ensure: Decrypted image
1: Compute $decrypted\_image \leftarrow encrypted\_image \oplus key$
2: Compute $inverse\_permutation \leftarrow argsort(permutation)$
3: Apply $inverse\_permutation$ to rows of $decrypted\_image$
4: **return** $decrypted\_image$ =0

XI. CONCLUSION

The alternate system [2] represents a variant of Parrondo's paradox, also known as the switching strategy. In Parrondo's paradox, combining two distinct complex systems may yield a more straightforward system, such as *chaos*^{1} + *chaos*^{2}, resulting in order, or two simple systems combining to form a complex system, like *order*^{1} + *order*^{2}, leading to chaos. We applied this methodology to SPLM, utilizing two constants, μ, and β, and iterating through the process.

REFERENCES

[1] J. Almeida, D. Peralta-Salas, and M. Romera. "Can two chaotic systems give rise to order?", *Physica D: Nonlinear Phenomena*, vol. 200, no. 1-2, pp. 124–132, 2005.

[2] Deepak Kumar and Mamta Rani, "Alternated superior chaotic biogeography-based algorithm for optimization problems," *International Journal of Applied Metaheuristic Computing (IJAMC)*, vol. 13, no. 1, pp. 1–39, 2022.

[3] Mengjiao Wang, Mingyu An, Xinan Zhang, and Herbert Ho-Ching Iu, "Two-variable boosting bifurcation in a hyperchaotic map and its hardware implementation," *Nonlinear Dynamics*, vol. 111, no. 2, pp. 1871–1889, 2023.

[4] Ali Kanso and Nejib Smaoui, "Irregularly decimated chaotic map(s) for binary digits generations", *International Journal of Bifurcation and Chaos*, vol. 19, no. 4, pp. 1169–1183, 2009.

[5] Jaco F. Schutte, Jeffrey A. Reinbolt, Benjamin J. Fregly, Raphael T. Haftka, and Alan D. George, "Parallel global optimization with the particle swarm algorithm", *International Journal for Numerical Methods in Engineering*, vol. 61, no. 13, pp. 2296–2315, 2004.

[6] Xin Zhang, Dexuan Zou, and Xin Shen, "A novel simple particle swarm optimization algorithm for global optimization", *Mathematics*, vol. 6, no. 12, pp. 287, 2018.

[7] Thejas Haridas, S. D. Upasana, G. Vyshnavi, Malavika S. Krishnan, and Sishu Shankar Muni, "Chaos-based audio encryption: Efficacy of 2D and 3D hyperchaotic systems", *Franklin Open*, vol. 8, pp. 100158, 2024.

[8] Hassan Elkamchouchi, Wessam M. Salama, and Yasmine Abouelseoud, "New video encryption schemes based on chaotic maps", *IET Image Processing*, vol. 14, no. 2, pp. 397–406, 2020.

[9] Somaya Al-Maadeed, Afnan Al-Ali, and Turki Abdalla, "A new chaos-based image-encryption and compression algorithm", *Journal of Electrical and Computer Engineering*, vol. 2012, no. 1, pp. 179693, 2012.

[10] Wassim Alexan, Marwa Elkandoz, Maggie Mashaly, Eman Azab, and Amr Aboshousha, "Color image encryption through chaos and KAA map", *IEEE Access*, vol. 11, pp. 11541–11554, 2023.

[11] Hongjun Liu, Jian Liu, and Chao Ma, "Constructing dynamic strong S-Box using 3D chaotic map and application to image encryption", *Multimedia Tools and Applications*, vol. 82, no. 16, pp. 23899–23914, 2023.

[12] Delavar Zareai, Mohammadali Balafar, and Mohammadreza FeiziDerakhshi, "EGPIECLMAC: Efficient grayscale privacy image encryption with chaos logistics maps and Arnold Cat", *Evolving Systems*, vol. 14, no. 6, pp. 993–1023, 2023.

[13] Marcin Lawnik, Lazaros Moysis, and Christos Volos. "Chaos-based cryptography: Text encryption using image algorithms", *Electronics*, vol. 11, no. 19, pp. 3156, 2022.

[14] Dragan Lambić. "Security analysis and improvement of the pseudo-random number generator based on piecewise logistic map", *Journal of Electronic Testing*, vol. 35, no. 4, pp. 519–527, 2019.

[15] Yong Wang, Zhaolong Liu, Jianbin Ma, and Haiyuan He, "A pseudo-random number generator based on piecewise logistic map", *Nonlinear Dynamics*, vol. 83, pp. 2373–2391, 2016.

[16] J. L. Fan and X. F. Zhang, "Piecewise logistic chaotic map and its performance analysis", *Acta Electronica Sinica*, vol. 37, no. 4, pp. 720–725, 2009.

[17] Ali Kanso and Nejib Smaoui, "Irregularly decimated chaotic map(s) for binary digits generations", *International Journal of Bifurcation and Chaos*, vol. 19, no. 4, pp. 1169–1183, 2009.

[18] Yong Wang, Zhaolong Liu, Jianbin Ma, and Haiyuan He, "A pseudo-random number generator based on piecewise logistic map", *Nonlinear Dynamics*, vol. 83, pp. 2373–2391, 2016.

[19] Yong Wang, Zhiqiang Zhang, Guodong Wang, and Dong Liu, "A pseudorandom number generator based on a 4D piecewise logistic map with coupled parameters", *International Journal of Bifurcation and Chaos*, vol. 29, no. 9, pp. 1950124, 2019.

[20] Sota Eguchi, Takeru Miyazaki, Shunsuke Araki, Satoshi Uehara, and Yasuyuki Nogami, "A study on randomness of sequences obtained from piecewise logistic map over integers", *2020 International Symposium on Information Theory and its Applications (ISITA)*, pp. 451–455, 2020.

[21] Tao Xiang, Xiaofeng Liao, and Kwok-wo Wong, "An improved particle swarm optimization algorithm combined with piecewise linear chaotic map", *Applied Mathematics and Computation*, vol. 190, no. 2, pp. 1637–1645, 2007.

[22] Nuo Jia and Tao Wang, "A GCM neural network with piecewise logistic chaotic map", *Symmetry*, vol. 14, no. 3, pp. 506, 2022.

[23] Narayan Partap and Renu Chugh, "Fixed point iterative techniques—an application to fractals", *International Journal of Research in Mathematics & Computation*, vol. 4, no. 1, pp. 1–7, 2016.

[24] Anju Yadav and Mamta Rani, "Modified and extended logistic map in superior orbit", *Procedia Computer Science*, vol. 57, pp. 581–586, 2015.

[25] Robert C. Hilborn, *Chaos and Nonlinear Dynamics: An Introduction for Scientists and Engineers*, Oxford University Press, 2000.

[26] Hossein Pishro-Nik, *Introduction to Probability, Statistics, and Random Processes*, Kappa Research, LLC, Blue Bell, PA, USA, 2014.

[27] Mohamad Ayob, Ahmad Faisal, Sundarapandian Vaidyanathan, Aceng Sambas, Khaled Benkouider, Mohd Kamal Mohd Nawawi, Kamal Khalid, and Elissa Nadia Madi, "Electronic Circuit in the Two-Scroll Hyperchaotic System with a Unique Saddle-Point Rest Point and its Synchronization via Integral Sliding Mode Control", *IAENG International Journal of Applied Mathematics*, vol. 54, no. 3, pp. 452–464, 2024.

[28] Yang Peng and Yuming Feng, "Impulse synchronization strategy of nonlinear finance systems", *IAENG International Journal of Applied Mathematics*, vol. 54, no. 9, pp. 1814–1819, 2024.

[29] Maie Aboghazalah, Passent El-Kafrawy, Abdelmoty M. Ahmed, Rasha Elnemr, Belgacem Bouallegue, and Ayman El-Sayed, "Arrhythmia detection by using chaos theory with machine learning algorithms", *Computers, Materials & Continua*, vol. 79, no. 3, pp. 3856–3875, 2024.

[30] Ziwei Liang, Shaobo He, Huihai Wang, and Kehui Sun, "A novel discrete memristive chaotic map", *The European Physical Journal Plus*, vol. 137, no. 3, pp. 1–11, 2022.

[31] Xiao-Yue Yao, Xian-Feng Li, Jun Jiang, and Andrew Y. T. Leung, "Codimension-one and -two bifurcation analysis of a two-dimensional coupled logistic map", *Chaos, Solitons & Fractals*, vol. 164, pp. 112651, 2022.

[32] Mehmet Şahin Açikkapi and Fatih Özkaynak, "A method to determine the most suitable initial conditions of chaotic map in statistical randomness applications", *IEEE Access*, vol. 9, pp. 1482–1494, 2020.

[33] Yong Wang, Zhaolong Liu, and Peng Lei, "Cryptographic properties analysis of piecewise logistic map", *Proceedings of the 2014 International Symposium on Nonlinear Theory and its Applications (NOLTA2014)*, pp. 393–396, 2014.

[34] Hadjer Bourekouche, Samia Belkacem, and Noureddine Messaoudi, "Randomness evaluation of coupled chaotic maps via NIST tests: A comparative study", pp. 25, 2023.

[35] Juan Wang, Yihai Wang, Xin Wen, Taiheng Yang, and Qun Ding, "The simulation research and NIST test of binary quantification methods for the typical chaos", *2015 Third International Conference on Robot, Vision and Signal Processing (RVSP)*, pp. 180–184, 2015.